Modeling LightInduced Synaptic Behavior and Visual Memory of Azopolymeric Compounds

Advanced Optical Materials

ADVANCED OPTICAL MATERIALS
www.advopticalmat.de

RESEARCH ARTICLE OPEN ACCESS

Modeling Light-Induced Synaptic Behavior and Visual Memory of Azopolymeric Compounds

Mateo Rosero-Realpe[1,2] | Federico Ferrarese Lupi[2] | Gianluca Milano[2] | Angelo Angelini[2]

[1]Department of Applied Science and Technology (DISAT), Politecnico di Torino, Torino, Italy | [2]Advanced Materials Metrology and Life Science Division, Istituto Nazionale di Ricerca Metrologica (INRiM), Torino, Italy

Correspondence: Mateo Rosero-Realpe (mateo.rosero@polito.it) | Angelo Angelini (a.angelini@inrim.it)

Received: 13 February 2026 | **Revised:** 22 June 2026 | **Accepted:** 25 June 2026

Keywords: azopolymers | light-responsive materials | neuromorphic computing | synaptic plasticity | visual memory

ABSTRACT

Adaptive and intelligent matter is becoming a cornerstone in the development of unconventional computing paradigms, as it allows to process and store information at the matter level in a way similar to biological neuronal systems. A crucial requirement for testing the implementation of neuromorphic-type of data processing is the ability to model and predict the material response under different stimulation conditions. In this work, we develop a modeling framework able to describe the dynamics of light-responsive organic materials when stimulated by light. By correlating parameters of a rate-balance based model with physical quantities, we highlight the basic mechanisms concurring to the temporal evolution of the material's internal state. The model accurately predicts the response to timely correlated signals, capturing the typical synaptic-like behavior of the light responsive material and reveals the contribution to the observed dynamic of both long-term and short-term memory components. To further explore the potential of the model, we use a spatially distributed gray scale intensity pattern to stimulate the material and show that the model accurately captures the spatio-temporal evolution of the material's internal state, unveiling the potential for visual memory applications.

1 | Introduction

The attempt to develop artificial systems able to mimic biological intelligence has led in recent years to the design of *intelligent matter*, that is matter able to perceive, process, and adapt its internal state in response to external stimuli [1]. In this framework, stimuli-responsive materials are crucial to develop novel concepts of hardware platforms that implement new computing paradigms beyond Von Neumann. In the realm of Internet of Things, for example, the ability of the sensing unit to pre-process information without exchanging data with the processing unit (in-sensor computing) reduces data transfer and computation complexity [2]. Also, adaptive materials exploiting intrinsic dynamics when subjected to external stimulation can be exploited for the physical implementation of novel computing paradigms, such as reservoir computing. In physical reservoir computing, the dynamics of a physical system endowing high nonlinearity and short-term memory are exploited to project the input signal into a higher dimensional space that is then analyzed by a readout layer [3]. Since the readout is the only part of the system to be trained, this computing paradigm is usually associated with reduced training costs. In this context, significant efforts have been made to develop hardware platforms with rich nonlinear dynamics, such as memristors based on anomalous phase transitions in $SbSe_x$ [4] or optoelectronic memories utilizing MoS_2 [5] heterojunctions for dual-mode (Short Term and Long Term Memory) operation.

Recently, it has been demonstrated that intrinsic dynamics of neuromorphic light-responsive organic materials can be exploited for physical reservoir computing [6]. These materials, in which the

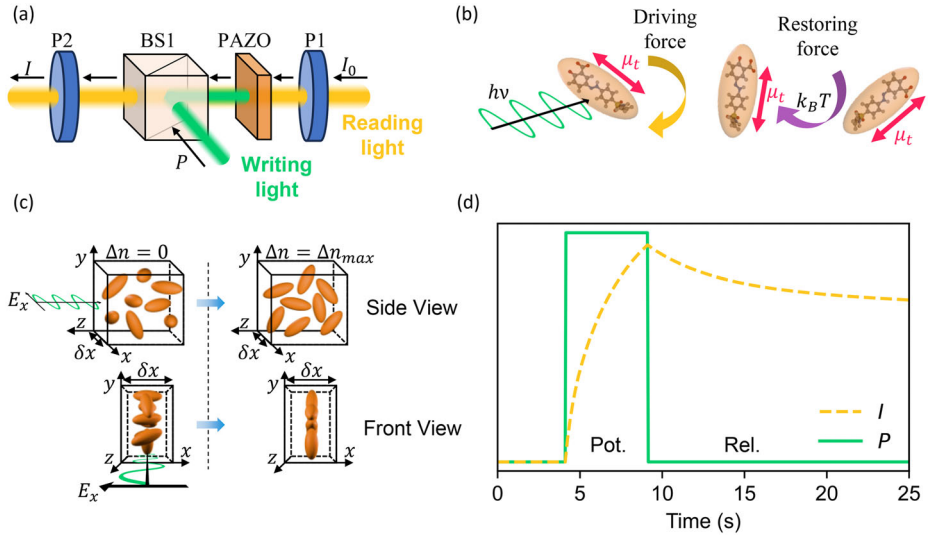

FIGURE 1 | (a) Simplified experimental configuration showing the Reading process via a white light source (I_0) through crossed polarizers (P1 and P2), the Writing process using a green laser ($\lambda = 520nm$) to stimulate the material (P). The simultaneous Writing + Reading mode is used to monitor the output intensity I while irradiating the sample. (b) Sketch of the molecular dynamics highlighting the competition between the Driving force, and the Restoring force.(c) Side and front views of the material volume illustrating the transition from an initial isotropic state ($\Delta n = 0$) to a saturated birefringent state ($\Delta n = \Delta n_{max}$) due to a stable preferential orientation of the molecules long axis perpendicular to the incident electric field $\vec{E}$. (d) Typical potentiation (Pot.) and relaxation (Rel.) dynamics of the reading light (I) when the material is stimulated with writing light (P).

adaptiveness resulting from the optically induced birefringence enables the emulation of a wide range of synaptic functionalities, have demonstrated to enable implementation of the physical reservoir computing paradigm by exploiting their nonlinear response with short-term memory dynamics. However, a model able to describe the dynamics of these systems for predicting outputs under specific light illumination, as required to test in silico the implementation of computing paradigms in these systems, is actually missing.

In this work, we report on a modeling framework able to describe optically induced neuromorphic dynamics of azopolymeric compounds. We show that experimental results can be explained in terms of two physical mechanisms acting on different timescales, and according to literature we attribute them to the fast reorientation of the azopolymeric group and the slow reorientation of the polymeric backbone, respectively [7] each described through a rate-balance equation. It is worth noticing here that there is still not complete agreement on the microscopic nature of the mechanisms underlying the induced birefringence in literature (see, for example [8] and [9]), although it is commonly accepted that different mechanisms acting on different timescales contribute to it. The combination of these two rate-balance equations, where equation parameters are directly correlated with key physical variables, is found to be able to quantitatively interpolate experimental data, providing a physic-based modeling framework for predicting the material response to arbitrary input light signals.

2 | Mechanism of Light-Induced Synaptic Plasticity

One of the approaches to emulate the synaptic behavior in azopolymeric systems [10–12] relies on the control of light-induced birefringence [13], a phenomenon that allows the material to "sense" and "remember" optical stimuli. To characterize the material response, we employ the optical configuration shown in Figure 1a (full experimental setup in Figure S1). The sketch shows two concurrent processes: the "reading" of the material's internal state and the "writing" of information. Reading is performed using a broadband white light source (Figure S2a) of intensity. I_0 passing through a pair of crossed linear polarizers (P1 and P2). In the initial isotropic state, no light reaches the detector ($I \approx 0$). Writing (or stimulation) is achieved using a continuous wave linearly polarized green laser ($\lambda = 520\ nm$), which induces molecular reorientation (Figure 1b) and, consequently, macroscopic birefringence, allowing light to pass through the analyzer (details on the experimental setup in Methods section and Note S1). In opposition to the laser driving force, the thermal motion tends to restore the pristine random orientation of the molecules, thus reducing the induced anisotropy and the overall birefringence.

This experimental approach allows us to observe the intrinsic dynamics of poly[1-[4-(3-carboxy-4-hydroxyphenyl-azo) benzene sulfonamido]-1,2-ethanediyl, sodium salt] (PAZO) films. The dynamics of this response follows an increment of the signal (potentiation) when exposed to laser stimulation and a decrease of the signal after the laser has been turned off (relaxation) as shown in Figure 1d, effectively encoding the history of the stimuli into the material's internal state.

To provide a physical basis for the modeling framework presented in the next section, we assume based on experimental evidences that the observed dynamics can be decomposed into two distinct physical mechanisms [7, 9, 14]: *i)* the azopolymeric group reorientation (fast mechanism) and *ii)* the polymeric backbone reorientation (slow mechanism). These two mechanisms acting on different timescales can be exploited to emulate rapid and

slow synaptic enhancement effects observed in certain types of biological synapses [15].

2.1 | Azopolymeric Group Reorientation—Fast Mechanism

Azobenzene derivatives act as molecular switches because they can exist in two distinct geometric isomeric forms: trans and cis [16]. In their stable trans state, they possess a rod-like structure [17] with a transition dipole moment (μ_t) parallel to their long axis [18]. Under laser illumination, these groups undergo repeated trans-cis-trans isomerization cycles. Since the probability of absorption follows $P_{abs}(\theta) \propto cos^2(\theta)$ [16], molecules with (μ_t) aligned with the electric field $\vec{E}$ are preferentially excited and reoriented until they fall into a "dark state" perpendicular to the polarization (Figure 1c), a phenomenon also known as orientational hole-burning [19, 20]. This process is relatively fast and governs the initial rapid rise and decay of the signal.

2.2 | Polymeric Backbone Reorientation—Slow Mechanism

As the azopolymeric side-groups reorient, they exert mechanical stress on the main polymeric backbone to which they are covalently bonded [13]. The backbone eventually undergoes a slower, cooperative reorientation to accommodate the new distribution of the azo-groups. This second mechanism contributes to a more stable, long-term component of the induced birefringence and relaxes much more slowly once the light is turned off due to the strong restrictions on molecular mobility and the structural impediments of the chain.

It is important to know that the macroscopic physical observable, the photoinduced birefringence (Δn), is an inherently continuous variable. This analog response emerges from the collective behavior of the molecular ensemble; the net birefringence depends on the statistical distribution and orientation of millions of chromophores and polymeric chains within the matrix.

This dual-nature response (a fast molecular component and a slow structural component) provides the physical justification for our double rate-balance equation model. Each mechanism is governed by its own potentiation k_p and relaxation k_d rates, directly linked to the electromagnetic driving force and the thermal restoring force, that is thermally activated rotational motion [16], respectively.

The relaxation dynamic can be eventually shortened by illuminating the sample with circularly polarized light that randomizes the molecular orientation [6].

It is worth noting that our modeling framework is applied in a phenomenological manner. Our model focuses on capturing the overall macroscopic response to enable in-silico predictions regardless of the underlying microscopic complexity.

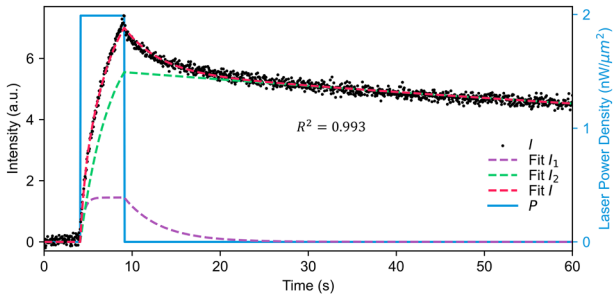

FIGURE 2 | Temporal evolution of the reading light intensity I when the material is stimulated by an optical pulse ($t_{on} = 5s\, P = 1.99nW/\mu m^2$). The black dots are the experimental data, while the blue line indicates the optical stimulation. The red dashed line corresponds to the model output (fit of I), which results from the combination of the two constituent terms: the fast component (I_1, purple dashed line) and the slow component (I_2, green dashed line).

3 | Modeling

The total transmitted light intensity I (physical observable) was modelled as the contribution of two independent terms related to the two involved mechanisms:

$$I = I_1 + I_2 \tag{1}$$

where I_1 and I_2 refer to the transmitted light intensity associated to the fast and slow mechanisms, respectively. This equation can be rewritten as:

$$I = I_{max,1} \cdot g_1 + I_{max,2} \cdot g_2 \tag{2}$$

where $I_{max,1}$ and $I_{max,2}$ are the maximum transmitted intensities corresponding to the case where all the azobenzene groups and the polymeric backbones are aligned, respectively, while g_1 and g_2 are the normalized internal state of the system indicating the percentage of molecules that are aligned. When $g_1 = 1$ (all azobenzene groups aligned), the transmitted intensity related to this mechanism is $I_{max,1}$, when $g_2 = 1$ (all polymeric backbones are aligned), the transmitted intensity related to this mechanism is $I_{max,2}$.

The evolution of the system is therefore modeled as the evolution of the two internal states of the system g_1 and g_2 each independently evolving according to a rate-balance equation [21, 22] (Note S2 for details):

$$\frac{dg_i}{dt} = k_{p,i} \cdot (1 - g_i) - k_{d,i} \cdot g_i \tag{3}$$

where $i = 1, 2$ and $k_{p,i}$ and $k_{d,i}$ represent potentiation and relaxation rate. By modeling the evolution of these populations rather than individual molecular transitions, the framework captures the continuum of internal states necessary for emulating synaptic-like weight modulation in the analog domain. Figure 2 shows the experimental data (black dots) representing the light intensity I transmitted under a pulsed stimulation P (blue line), while the red dashed line is the output of the fitting procedure.

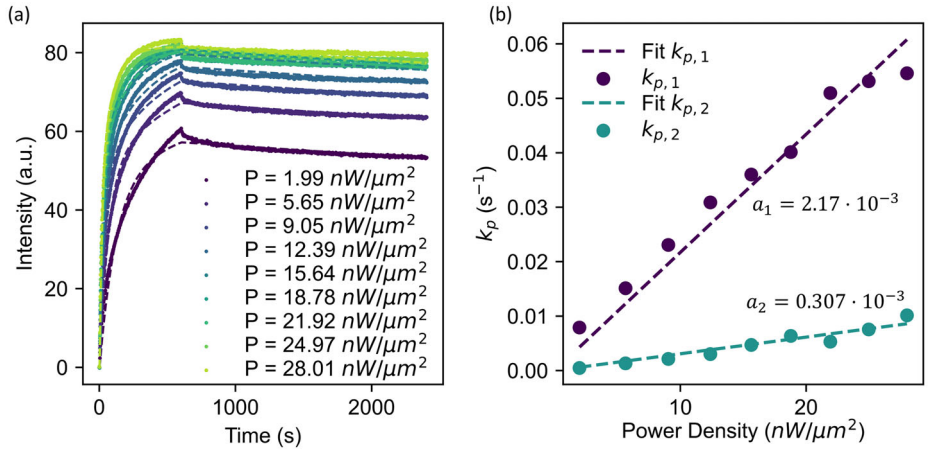

FIGURE 3 | Dependence of the photoinduced birefringence on P. (a) Reading light intensity measured for different power densities and fixed pulse duration ($t_{on} = 600s$). Experimental data (scattered dots) and corresponding model fits (solid lines) are shown for power densities ranging from $1.99nW/\mu m^2$ to $28.01nW/\mu m^2$ (bottom to top). (b) Potentiation rates $k_{p,1}$ (purple dots) and $k_{p,2}$ (teal dots) extracted from the global fit as a function of the power density. The dashed lines represent linear fits, confirming that the molecular reorientation rates scale proportionally with the incident light intensity.

Since the reading light is polarized as well, we evaluated the influence of it on the system dynamics and found it to be negligible in our experimental conditions (Figure S3). The two components of the rate balance equation are also plotted as green and purple dashed lines respectively. For comparison, Figure S4 reports the fitting result using a single rate balance equation. The rate-balance equation, that can be solved analytically following a recursive approach (Methods), has been exploited for modeling temporal dynamics of memristors, i.e. resistors with memory, where the internal state is represented by the device conductance and dynamics relies on the formation and rupture of nanoscale conductive filaments [21–23]. Also, a rate-balance equation has been exploited for modeling synaptic dynamics of a 2D memitter, i.e., an emitter with memory, where the internal state is represented by the stimuli-responsive photoluminescence [24].

In our work, the potentiation rates were considered to be linearly dependent on the power illumination P according to the relation:

$$k_{p,i} = \alpha_i \cdot P \tag{4}$$

Where α_i is a scalar coefficient representing the line slope.

The choice of a linear dependence of $k_{p,1}$and $k_{p,2}$ on P is related to the mechanism of optical absorption in azobenzene compounds. In these materials, molecular reorientation occurs because the chromophores undergo trans-cis isomerization upon absorbing photons. As demonstrated in the mean-field theory, the temporal evolution of the birefringence depends linearly on the incident irradiation through a coefficient which incorporates material-specific properties such as the absorption cross-section, quantum efficiency, and the initial order parameter [25].

The relaxation rates were considered to be dependent on temperature T according to an Arrhenius relations [26]:

$$k_{d,i} = A_i \, e^{\frac{E_{a,i}}{k_B T}} \tag{5}$$

where $i = 1, 2$ and $E_{a,i}$ is the activation energy related to each mechanism, while k_B is the Boltzmann constant.

The choice of an Arrhenius type for describing the dependence of $k_{d,1}$and $k_{d,2}$ on T is related to the assumption that the restoring force is a thermally activated phenomenon, responsible for reorienting the molecules toward an isotropic configuration.

3.1 | Potentiation Rate and Power Density

The dependence of k_p versus the power density was investigated by acquiring the response of the material to light stimulations with different power amplitudes. By keeping a fixed $k_{d,i}$ (i.e., by stimulating at constant temperature) and a constant $I_{max,i}$ for all curves, Figure 3a reports the temporal profiles of PAZO dynamics as the pump power density P varies from $1.99nW/\mu m^2$ to $28.01nW/\mu m^2$ over a 10-min stimulation period. This approach allowed for a global fit over the nine experimental curves, specifically correlating the potentiation parameters $k_{p,i}$ with the external driving force. As shown in Figure 3b, the relationship between $k_{p,i}$ and P is well-described by a linear fit within the investigated range, confirming that the rate of the molecular reorientation scales proportionally with the incident light intensity. The relation between the incident light intensity and the potentiation has been also reported in a recent paper from our group [6], where we analyzed the transition from short term to long term memory due to different experimental conditions (pulse intensity, duration, number of pulses).

3.2 | Relaxation Rate and Temperature

The dependence of k_d on temperature was investigated by acquiring the material response to a fixed light stimulation (pump power density $10nW/\mu m^2$, stimulation duration (10 s) at 8 different temperatures (Figure 4a), while fixing all the other parameters. The figure shows a clear trend, where the photoinduced birefringence

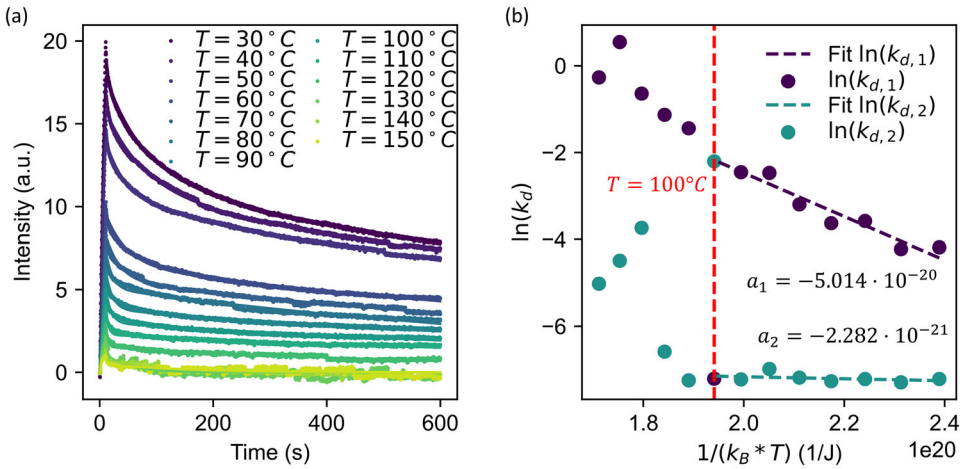

FIGURE 4 | Temperature dependence of the birefringence relaxation dynamics. (a) Reading light Intensity I measured at different temperatures, ranging from 30°C to 150°C (top to bottom) and fixed writing pulse ($t_{on} = 10s, P = 10nW/\mu m^2$). Experimental data (scattered dots) and global model fits (solid lines) illustrate the accelerated relaxation of the internal state as temperature increases. (b) Natural logarithm of the relaxation rates $k_{d,1}$ and $k_{d,2}$ as a function of $1/(k_B T)$. The dashed lines represent the linear fits from 30°C to 90°C, correlating the relaxation mechanisms with thermally activated rotational Brownian motion according to the Arrhenius law. The vertical red line divides the data at temperatures above (right side of the figure) and below (left part of the figure) the T_g.

drops down as the temperature increases. In the fitting procedure, to explicit the dependence of $k_{d,i}(T)$ we fixed a constant value of the parameter $G_{max,i}$ for all the curves, and analyzed how $k_{d,i}$ varies with respect to the temperature. In this case $k_{p,i}$ is a local parameter and its dependence on the temperature is shown on Figure S3. Figure 4b shows the relation between $k_{d,i}$ from T, confirming that in the range of temperatures considered the relaxation rate follows Equation (5). In particular, the fast component has a linear coefficient of $5.014x10^{-20}$, while the linear coefficient of the slow component is one order of magnitude lower ($2.282x10^{-21}$).According to the Arrhenius law, the slopes found in the linear fits represent the activation energies of the restoring processes. We underline here that the validity of the found relation is limited to Temperatures below the PAZO glass transition temperature $T_g \approx 100°C$ [27].

4 | Paired Pulse Facilitation

The light-induced modulation of the azopolymeric compound's internal state discussed in the previous sections can be inherently interpreted as a form of synaptic plasticity. Specifically, the variation in the material's response following a single optical stimulus represents a change in synaptic weight. By leveraging this history-dependent internal state, the system can emulate complex neuromorphic functionalities typical of biological synapses' short-term memory (STM). A fundamental manifestation of this behavior is the Paired-Pulse Facilitation (PPF) [28], where the synaptic response to a second stimulus is enhanced by the residual effect of a preceding one.

While the proposed model accurately predicts the material's response to single pulses at various temperatures and power densities, advanced computational frameworks—such as neuromorphic and reservoir computing—require precise modeling of system dynamics under temporally correlated stimuli (for PPF) [29].

To demonstrate the capability of the model to predict the system dynamics under temporally correlated stimuli (as for the PPF), we show the material's response to a sequence of ten optical pulses (blue line, $t_{on} = 1s$, $t_{off} = 1s$) with a power density of $1.99nW/\mu m^2$ (Figure 5). The experimental data (black dots) exhibit the characteristic synaptic-like behavior, where the signal undergoes progressive potentiation during the pulse train. By applying the double rate-balance equation, the model (red dashed line) successfully captures the complex evolution of the internal state.

The decomposition into fast (I_1, purple) and slow (I_2, green) components reveals how the short-term and long-term dynamics contribute to the overall response. The two terms integrate the history of the stimuli, providing the memory effect essential for reservoir computing. Notably, this framework provides a significantly better fit to the experimental dynamics compared to a single rate-balance equation (Figure S4), which fails to account for the multi-scale relaxation.

We then characterized the material's response to paired-pulse stimulation at varying inter-pulse intervals (t_{off}). The PPF ratio was quantified by calculating the relative amplitude of the second response (A_2) compared to the first (A_1), expressed as (A_2/A_1)*100%. Figure 5b illustrates the evolution of the PPF ratio as a function of t_{off}, clearly demonstrating the expected inverse relationship where the facilitation effect decays as the interval between stimuli increases. To ensure the robustness of our modeling framework, a global fit was performed across the entire set of experimental curves for different t_{off} values to extract the internal parameters that best describe the underlying dynamics (details in methods). The results of the global fit for every curve are shown in Figure S7. As shown in Figure 5b, there is excellent agreement between the experimental data and the fitted model, confirming that the double rate-balance equation effectively captures the temporal correlation and memory traces within the azopolymeric compound.

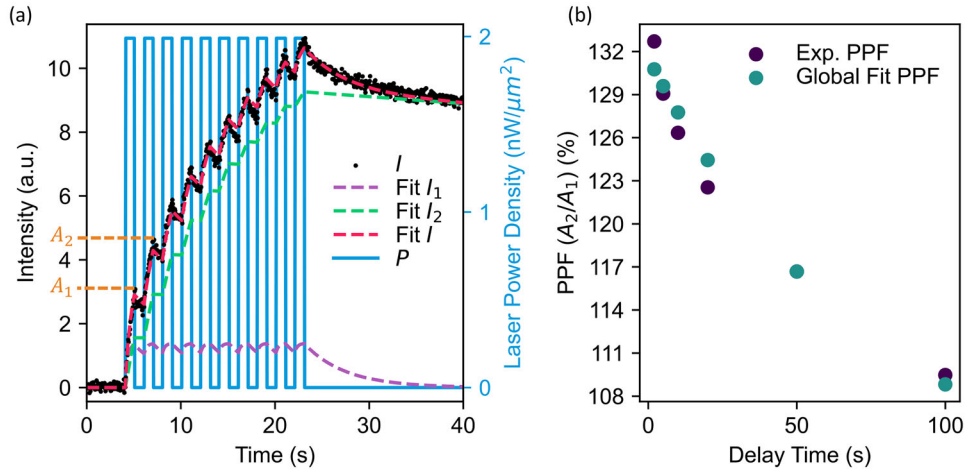

FIGURE 5 | (a) Experimental transmitted intensity (black dots) during and after a sequence of ten optical pulses (blue line; $t_{on} = 1s$, $t_{off} = 1s$) at a power density of $1.99nW/\mu m^2$. The double rate-balance equation model (red dashed line) accurately predicts the progressive potentiation of the internal state ($R = 0.997$). The total response is decomposed into the fast component (I_1, purple dashed line) and the slow component (I_2, green dashed line). (b) Experimental and fitted PPF percentages for different t_{off} ($P = 8.3nW/\mu m^2$, $t_{on} = 500ms$).

Consequently, these model parameters enable the in silico prediction of synaptic responses for arbitrary stimulation variables, such as pulse duration (t_{on}) and interpulse intervals (t_{off}). This predictive power allows for the optimization of experimental conditions for specific computational tasks without the need for exhaustive real-world characterization.

5 | Visual Memory

In our previous work [6], we demonstrated that PAZO can be used to emulate visual memory by storing spatially distributed intensity patterns that mimic the persistence of images on the human retina. Additionally, the material's adaptive nature enables motion perception, allowing it to detect and reconstruct the spatiotemporal history of moving objects by analyzing the continuous memory traces and fading dynamics left within the physical substrate.

In this work, we extend these capabilities by utilizing an analog input pattern rather than a binary "on/off" stimulus. By modulating the laser irradiation, we implement a grayscale representation where information is encoded in the intensity of the light. As shown in Figure 6a, the initial spatial distribution is an 8-bit grayscale bitmap, where each pixel's value (0 to 255) represents a specific information level. These values are mapped to a power percentage scale, where 255 corresponds to 100% ($P_{max} = 9.52nW/\mu m^2$) and 0 corresponds to 0%. Using a Digital Micromirror Device (DMD), the incident laser light is spatially and temporally modulated to match this percentage map (details in the Methods section).

Figure 6b illustrates the system's response when the PAZO film is exposed to this grayscale pattern for a pulse duration of $t_{on} = 10s$. Upon turning the laser off, the output intensity recorded by the camera reveals the relaxation dynamics of the stored image (Experimental Data). To replicate this behavior numerically, we modeled each pixel as an independent dynamical unit. The model was calibrated using the dynamics of a region exposed to P_{max} to ensure accurate fitting. The intensity $I_{x,y}$ for each pixel follows the double rate balance Equation (6):

$$I_{x,y} = I_{max,1} \cdot g_{x,y,1} + I_{max,2} \cdot g_{x,y,2} \tag{6}$$

While the fitting parameters remain consistent across the film, the potentiation rate constant $k_{p,x,y,i}$ is scaled according to the local power percentage:

$$k_{p,x,y,i} = \alpha_i \cdot P\%_{x,y} \tag{7}$$

where α_i represents the value of $k_{p,x,y,i}$ at 100% power density irradiation (P_{max}). This approach demonstrates that the inherent molecular dynamics of PAZO can faithfully process and retain complex, non-binary visual information in the analog domain. It also demonstrates that at macroscopic level, the dynamics of a film can be approximated to a matrix of single contributions.

6 | Conclusions

In this work, we propose a rate balance equation model to describe the potentiation and relaxation dynamics of optically induced birefringence in a commercial azopolymeric material (PAZO). The behavioral model accurately captures the synaptic-like response of the material, which is a crucial functionality for hardware neuromorphic computing. We find that our model achieves a high accuracy ($R^2 = 0.993$) in describing the experimental data.

By analyzing the correlation of the model's parameters with experimental ones we established a quantitative physical interpretation that describes the driving and restoring forces: the relaxation rate parameters $k_{d,i}$ are shown to obey the Arrhenius law, confirming their dependence on thermally activated rotational Brownian motion, the primary restoring force in the system, while the potentiation rate parameters $k_{p,i}$ are found to exhibit a linear dependence on the incident pump laser power density P, correlating them directly to the electromagnetic driving

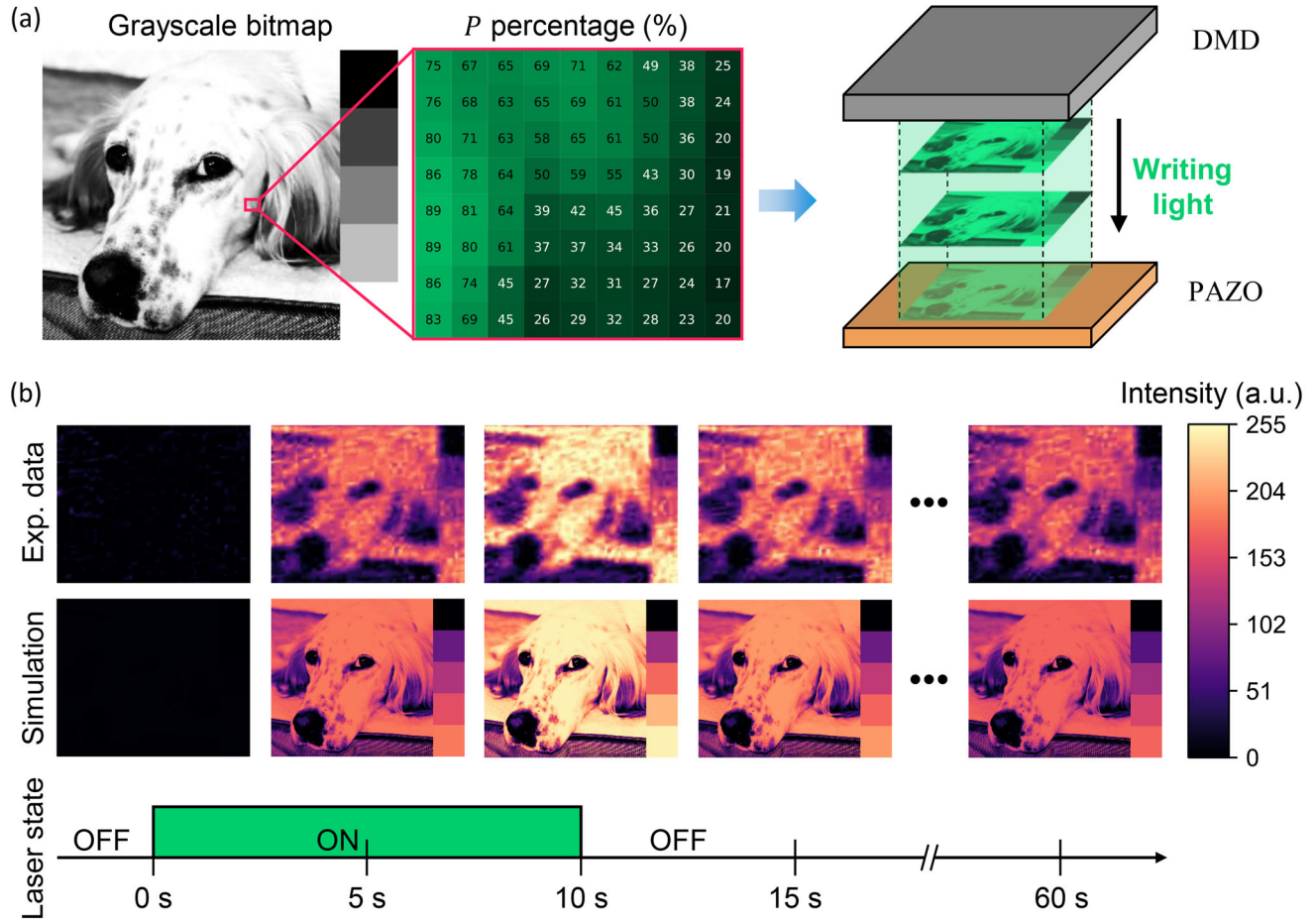

FIGURE 6 | (a) Mapping of an 8-bit grayscale bitmap (original picture taken by the authors) into a power percentage map ($P\%$) for spatial light modulation via DMD. (b). Spatiotemporal evolution of the output signal during and after a $t_{on} = 10s$ pulse, comparing experimental data (upper sequence) and the model output (lower sequence) under the same stimulation conditions (bottom line indicating the laser state). The relaxation dynamics demonstrate that each pixel, acting as an independent dynamical unit, can store and process analog information.

force. We highlight here that a comprehensive description of the underlying microscopic phenomena associated with the potentiation and relaxation dynamics of light induced birefringence is still not completely clear in literature, and different explanations have been provided [8, 9]. However it is well established that different mechanisms acting on different timescales concur to the effect. The relevance of our model is that it captures the overall macroscopic dynamic response and allows us to predict the evolution of the material's internal state under different experimental conditions regardless of the specific microscopic mechanisms.

Notably, the behavioral model developed describes the response to temporally correlated optical pulses, a key requirement for advanced computational paradigms like reservoir computing. In addition, we show that the model successfully captures the temporal evolution of spatially distributed grayscale intensity patterns, revealing the potential to predict the storage and processing of information associated with extended images. In addition, the model allows prediction of the material's response under arbitrary stimulation waveforms, which can be relevant in computational tasks where an analog input is applied. The ability to correlate model parameters with physical variables provides a powerful tool for the rational design and optimization of light-responsive organic materials for specific neuromorphic applications, paving the way for more energy-efficient and scalable hardware implementation of artificial intelligence.

7 | Methods

7.1 | Sample Preparation

For the sample preparation, we followed the procedure described in a previous work [6]. The absorption spectrum of PAZO and the result of the spin-coating method is shown in Figure S2b.

7.2 | Optical Setup

A continuous-wave linearly polarized laser emitting at 520 nm is used as the writing light. The polarization direction is oriented at 45° with respect to the orientation of P1 and P2. P1 and P2 are oriented perpendicular to each other.

The extended image in Figure 6 has been projected on the sample using a DMD (DLP6500 from Texas Instrument). The intensity

distribution is obtained by temporally modulating the signal via a Pulse Width Modulation where the total period is 2.78 ms.

7.3 | Mathematical Modeling and Numerical Implementation

The temporal evolution of g was modeled using a first-order linear ordinary differential equation (ODE) defined as $dg/dt = k_p\,(1-g) - k_d g$. To facilitate numerical simulation, the ODE was analytically solved using the method of separation of variables. By integrating the expression over a discrete time interval $[t-\Delta t,\ t]$, the following recursive analytical solution was obtained:

$$g\ (t) = \frac{k_p}{k_p + k_d} + \left(g\,(t-\Delta t) - \frac{k_p}{k_p + k_d} \right) \cdot e^{-(k_p + k_d)\cdot \Delta t} \tag{8}$$

The rate balance equation model was implemented in python by initializing the value of $g_i[0] = 0$ and calculating the next values iteratively following Equation (8). The values of $k_{d,i}$ remain constant in every time step, while, $k_{p,i}$ is multiplied by a binary variable having values of 0 or 1, depending on whether the pump laser is off or on, respectively.

To perform the global fit at different power densities or different temperatures, a specific code is used. For all the curves that we may fit, we can define global or local fitting parameters ($k_{p,1}$, $k_{d,1}$, $I_{max,1}$, $k_{p,2}$, $k_{d,2}$, $I_{max,2}$). The global ones will be shared by all the curves, while the local ones will be specific for each curve. In Figure 2, the global parameters are $I_{max,1}$ and $I_{max,2}$, while the local ones are $k_{p,1}$, $k_{d,1}$, $k_{p,2}$ and $k_{d,2}$. In Figure 3, the global parameters are $k_{d,1}$, $I_{max,1}$, $k_{d,2}$ and $I_{max,2}$, while the local parameters are $k_{p,1}$ and $k_{p,2}$. In order to perform the fitting in this way, we constructed a function that concatenates the result of calculating the I function for every curve (vector 1) and concatenates the experimental signal for every curve (vector 2), and used the function curve_fit included in the package scipy to reduce the value of the loss function (least squares) for these two vectors (See information about the convergence in Supplementary Note N3). The amount of parameters to fit will follow the next Equation (9):

$$N_{fit} = N_{global} + N_{local} \cdot n_{curves} \tag{9}$$

For the modeling of PPF, a global fitting procedure was implemented to simultaneously process experimental data across the entire range of inter-pulse intervals (t_{off}). In this approach, all model parameters were treated as global variables to ensure a consistent physical description of the material's dynamics across different temporal scales. Since all experiments were recorded with a fixed sampling period, the total number of data points naturally increases for curves with longer t_{off}. To prevent the loss function from being disproportionately weighted by these longer trials, a selective downsampling strategy was adopted to achieve a non-uniform temporal resolution. High resolution (one sample per sampling period) was maintained for regions in close temporal proximity to the laser pulses, where the fastest dynamics occur. Conversely, segments further from the pulses were downsampled by a factor that increased proportionally with the t_{off} value. This adaptive downsampling ensures that each experimental curve contributes equally to the global optimization process, regardless of its total duration.

7.4 | Visual Memory Implementation

To implement the visual memory experiments, the continuous-wave linearly polarized laser emitting was employed as the writing source. To ensure a homogeneous illumination and a constant power density across the active area, the gaussian laser beam was conditioned through spatial filtering and expansion; specifically, only the central and most uniform portion of the Gaussian profile was selected. This conditioned beam was then directed onto the DMD, consisting of an array of micro-mirrors capable of high-resolution spatial and temporal light modulation. The spatially modulated light reflected from the DMD was collected, filtered, and subsequently projected onto the PAZO film through a 5x objective lens. This optical configuration allowed for the precise "writing" of complex grayscale information into the material's internal state. The intensity levels were controlled by a Pulse Width Modulation (PWM) scheme with a total period of 2.78 ms, mapping the 8-bit grayscale values to a local power percentage scale. In the experiment, each pixel is treated as an independent element, as the spatial region on the PAZO sample associated with each pixel is much smaller than the characteristic length scale of molecular reorientation, and the cross-talk between adjacent pixels is neglected.

Funding

This work was financially supported by the Italian Ministry for Universities and Research under the Research Projects of National Relevant Interest (PRIN) project "Polymer mETAmateriaL for nanophotonicS (PETALS)" (grant no. 2020TS9LXS_004). G.M. acknowledges funding by the European Union (ERC, "MEMBRAIN", No. 101160604). Views and opinions expressed are however, those of the authors only and do not necessarily reflect those of the European Union or the European Research Council. Neither the European Union nor the granting authority can be held responsible for them. Part of this work was supported by the Italian Ministry of Health under the Piano Operativo Salute, project "RADIOAMICA" (CUP: H53C22000650006).

Conflicts of Interest

The authors declare no conflicts of interest.

Data Availability Statement

The data/code supporting the findings of this study are openly available in Zenodo at https://doi.org/10.5281/zenodo.21235244. All other data are available from the authors.

References

1. C. Kaspar, B. J. Ravoo, W. G. van der Wiel, S. V. Wegner, and W. H. P. Pernice, "The Rise of Intelligent Matter," *Nature* 594 (2021): 345–355, https://doi.org/10.1038/s41586-021-03453-y.

2. T. Wan, B. Shao, S. Ma, et al., "Sensor Computing: Materials, Devices, and Integration Technologies," *Advanced Materials* 35 (2023): 2203830, https://doi.org/10.1002/adma.202203830.

3. G. Tanaka, T. Yamane, J. B. Héroux, et al., "Recent Advances in Physical Reservoir Computing: A Review," *Neural Networks* 115 (2019): 100–123, https://doi.org/10.1016/j.neunet.2019.03.005.

4. G. Zhou, D. Gu, J. Ye, et al., "Anomalous Phase Change in $SbSe_X$ Memristors for Ultrafast Image Encryption," *Advanced Materials* 37 (2025): 08107, https://doi.org/10.1002/adma.202508107.

5. Y. Wang, L. Chen, B. Wu, et al., "Dual-Mode Optoelectronic Neuromorphic Memory for Complex Edge Detection and Recognition," *Advanced Functional Materials* 36 (2026): 14949, https://doi.org/10.1002/adfm.202514949.

6. F. Ferrarese Lupi, M. Rosero-Realpe, A. Ocarino, F. Frascella, G. Milano, and A. Angelini, "Neuromorphic Light-Responsive Organic Matter for in Materia Reservoir Computing," *Advanced Materials* 37 (2025): 2501813, https://doi.org/10.1002/adma.202501813.

7. A. Kozanecka-Szmigiel, K. Switkowski, E. Schab-Balcerzak, and D. Szmigiel, "Photoinduced Birefringence of Azobenzene Polymer at Blue Excitation Wavelengths," *Applied Physics B* 119 (2015): 227–231, https://doi.org/10.1007/s00340-015-6046-8.

8. O.-K. Song, C. H. Wang, and M. A. Pauley, "Dynamic Processes of Optically Induced Birefringence of Azo Compounds in Amorphous Polymers below Tg," *Macromolecules* 30 (1997): 6913–6919, https://doi.org/10.1021/ma9701649.

9. M. S. Ho, A. Natansohn, and P. Rochon, "Azo Polymers for Reversible Optical Storage. 7. The Effect of the Size of the Photochromic Groups," *Macromolecules* 28 (1995): 6124–6127, https://doi.org/10.1021/ma00122a020.

10. C.-R. Lee, Y.-C. Chung, and Y.-C. Hung, "Synaptic Plasticity and Light-Triggered Properties of Azo-Dye-Doped DNA Biopolymer Devices," *Organic Photonic Materials and Devices* 13363 (2025): 56–61.

11. Y. Wang, B. Han, M. Mayor, and P. Samorì, "Opto-Electrochemical Synaptic Memory in Supramolecularly Engineered Janus 2D MoS 2," *Advanced Materials* 36 (2024): 2307359, https://doi.org/10.1002/adma.202307359.

12. J. Tian, L. Fu, Z. Liu, et al., "Optically Tunable Field Effect Transistors with Conjugated Polymer Entailing Azobenzene Groups in the Side Chains," *Advanced Functional Materials* 29 (2019): 1807176, https://doi.org/10.1002/adfm.201807176.

13. A. Natansohn and P. Rochon, "Photoinduced Motions in Azo-Containing Polymers," *Chemical Reviews* 102 (2002): 4139–4176, https://doi.org/10.1021/cr970155y.

14. M. Raposo, Q. Ferreira, A. R. Monteiro Timóteo, P. A. Ribeiro, and A. M. B. do Rego, "Contribution of Counterions and Degree of Ionization for Birefringence Creation and Relaxation Kinetics Parameters of PAH/PAZO Films," *Journal of Applied Physics* 118 (2015): 114504, https://doi.org/10.1063/1.4930802.

15. R. S. Zucker and W. G. Regehr, "Short-Term Synaptic Plasticity," *Annual Review of Physiology* 64 (2002): 355–405, https://doi.org/10.1146/annurev.physiol.64.092501.114547.

16. Z. Sekkat, J. Wood, and W. Kn, "Reorientation Mechanism of Azobenzenes within the Trans. fwdarw. cis Photoisomerization," *The Journal of Physical Chemistry* 99 (1995): 17226–17234.

17. S. De Martino and P. A. Netti, "Dynamic Azopolymeric Interfaces for Photoactive Cell Instruction," *Biophysics Reviews* 1 (2020): 011302, https://doi.org/10.1063/5.0025175.

18. E. Blasco, M. Piñol, and C. Berges, "Smart Polymers for Optical Data Storage," in *Smart Polymers and Their Applications* (Elsevier, 2014), 510–548.

19. S. L. Oscurato, M. Salvatore, P. Maddalena, and A. Ambrosio, "From Nanoscopic to Macroscopic Photo-Driven Motion in Azobenzene-Containing Materials," *Nanophotonics* 7 (2018): 1387–1422, https://doi.org/10.1515/nanoph-2018-0040.

20. T. Buffeteau, F. Lagugné Labarthet, M. Pézolet, and C. Sourisseau, "Photoinduced Orientation of Azobenzene Chromophores in Amorphous Polymers As Studied by Real-Time Visible and FTIR Spectroscopies," *Macromolecules* 31 (1998): 7312–7320, https://doi.org/10.1021/ma980843z.

21. E. Miranda, G. Milano, and C. Ricciardi, "Modeling of Short-Term Synaptic Plasticity Effects in ZnO Nanowire-Based Memristors Using a Potentiation-Depression Rate Balance Equation," *IEEE Transactions on Nanotechnology* 19 (2020): 609–612, https://doi.org/10.1109/TNANO.2020.3009734.

22. G. Milano, F. Michieletti, D. Pilati, C. Ricciardi, and E. Miranda, "Self-Organizing Neuromorphic Nanowire Networks as Stochastic Dynamical Systems," *Nature Communications* 16 (2025): 3509, https://doi.org/10.1038/s41467-025-58741-2.

23. G. Milano, G. Pedretti, K. Montano, et al., "In Materia Reservoir Computing with a Fully Memristive Architecture Based on Self-Organizing Nanowire Networks," *Nature Materials* 21 (2022): 195–202, https://doi.org/10.1038/s41563-021-01099-9.

24. F. Ferrarese Lupi, G. Milano, A. Angelini, et al., "Synaptic Plasticity and Visual Memory in a Neuromorphic 2D Memitter Based on WS_2 Monolayers," *Advanced Functional Materials* 34 (2024): 2403158, https://doi.org/10.1002/adfm.202403158.

25. T. G. Pedersen and P. M. Johansen, "Mean-Field Theory of Photoinduced Molecular Reorientation in Azobenzene Liquid Crystalline Side-Chain Polymers," *Physical Review Letters* 79 (1997): 2470–2473, https://doi.org/10.1103/PhysRevLett.79.2470.

26. K. J. Laidler, "The Development of the Arrhenius Equation," *Journal of Chemical Education* 61 (1984): 494, https://doi.org/10.1021/ed061p494.

27. Q. Ferreira, P. A. Ribeiro, O. N. Oliveira, and M. Raposo, "Long-Term Stability at High Temperatures for Birefringence in PAZO/PAH Layer-by-Layer Films," *ACS Applied Materials & Interfaces* 4 (2012): 1470–1477, https://doi.org/10.1021/am201722x.

28. A. Citri and R. C. Malenka, "Synaptic Plasticity: Multiple Forms, Functions, and Mechanisms," *Neuropsychopharmacology* 33 (2008): 18–41, https://doi.org/10.1038/sj.npp.1301559.

29. G. Milano, M. Luebben, Z. Ma, et al., "Self-Limited Single Nanowire Systems Combining All-in-One Memristive and Neuromorphic Functionalities," *Nature Communications* 9 (2018): 5151, https://doi.org/10.1038/s41467-018-07330-7.

Supporting Information

Additional supporting information can be found online in the Supporting Information section.

Supporting File: adom71444-sup-0001-SuppMat.docx.